Modulation of Electrostatic Potential in 2D Crystal Engineered by an Array of Alternating Polar Molecules

Neno Fuller,[1,*] Fatimah Rudayni,[1,2] Stephanie Amos,[1] Kushal Rijal,[1] Seyed A. Maroufian,[1] Pavel Valencia-Acuna,[1] Tyson Karl,[1] Hui Zhao,[1] Hartwin Peelaers,[1,*] Qunfei Zhou,[1,*] Wai-Lun Chan[1,*]

1. Department of Physics and Astronomy, University of Kansas, Lawrence, Kansas 66045, US
2. Department of Physics, Jazan University, Jazan 45142, Saudi Arabia

[*]E-mail: fuller.neno@ku.edu, peelaers@ku.edu, qunfei.zhou@ku.edu, wlchan@ku.edu

Abstract:

The moiré potential in rotationally misfit two-dimensional (2D) heterostructures has been used to build artificial exciton and electron lattices, which have become platforms for realizing exotic electronic phases. Here, we demonstrate a different approach to create a superlattice potential in 2D crystals by using the near field of an array of polar molecules. A bilayer of titanyl phthalocyanine (TiOPc), consisting of alternating out-of-plane dipoles, is deposited on monolayer MoS_2. Time-resolved two-photon photoemission spectroscopy (TR-TPPE) reveals a pair of interlayer exciton (IX) states with an energy difference of ~ 0.1 eV, which is consistent with the electrostatic potential modulation induced by the TiOPc bilayer as determined by density functional theory (DFT) calculations. Because the symmetry and the period of this potential superlattice can be changed readily by using molecules of different shapes and sizes, molecule/2D heterostructures can be promising platform for designing artificial exciton and electron lattices.

Keywords: 2D heterostructures, organic molecules, excitons, electrostatic effects, photoelectron spectroscopy, density functional theory

2D van der Waals (vdW) heterostructures have attracted much attention recently because material properties can be engineered by stacking different 2D crystals together. One way to control properties is by forming a nanoscale periodic potential known as the moiré potential, which has been used to realize fractal quantum Hall effect[1-3] and unconventional superconductivity in bilayer graphene.[4] For type-II heterostructures formed by transition metal dichalcogenide crystals (TMDCs), electrons and holes are separated by the interface to form interlayer excitons (IXs). These IXs have very long lifetimes,[5] which enable the creation of spin and valley current.[6, 7] The emissive[8-12] and transport[13, 14] properties of the IXs can be further controlled by the moiré potential. Because excitons are bosons, moiré-trapped IXs can also be used to realize high-temperature Bose-Einstein condensates (BECs).[15] These novel electronic phases can have many potential applications. For example, both moiré-trapped excitons and BECs can be used for quantum information processing and quantum computation.[16-19]

Inorganic 2D crystals can also be combined with organic molecules to form hybrid type-II heterostructures.[20-22] IXs formed in these hybrid type-II heterostructures can have an even longer lifetime.[23] In addition, flexibilities and functionalities provided by molecules can provide unique tuning knobs for engineering exciton and carrier properties. For example, organic molecules can passivate defects in TMDCs.[24] The properties of molecules and TMDCs can influence each other to produce unusually high IX mobilities,[25] and nearly-free electron behavior in the organic layer.[26] Organic molecules can also enhance the photoluminescence yield of TMDCs through effective energy transfer.[27, 28] The electric field from organic molecules can create localized doping in 2D crystals, which can produce nanoscale lateral p-n junctions.[29, 30]

Previously, by combining various small molecules with TMDCs, we have shown that IX's dynamics can be influenced heavily by out-of-plane[31, 32] and in-plane[33] variations in the electron

potential energy. Here, we further showcase a nanoengineering approach enabled by an array of polar molecules. These molecules can produce a modulating electrostatic potential superlattice at the neighboring 2D crystal, which can be used to organize electrons spatially by localizing them in lower energy sites. Indeed, theoretical calculations[34] have already shown that the near field from a planar/quasi-planar molecular layer can create a modulating potential in a nearby graphene layer with a peak-to-peak amplitude as large as 0.5 eV. These periodic potentials would be used to create and stabilize artificial exciton and electron lattices such as Wigner crystals[35, 36] and Kagome lattices.[37] Compared to the moiré potential in 2D heterostructures, the periodic potential produced by molecular layers can be largely tuned in symmetry, period and magnitude by the shape, size and quadrupole moment of the organic molecule.[34] Because an extensive library of semiconducting molecules is already available, this method offers unprecedented opportunities to tailor exotic electronic and excitonic phases. Moreover, molecule/TMDC heterostructures can host a higher density of IXs, which can favor the formation of high-temperature BECs.[38]

To explore the impacts of a periodic array of molecular dipoles, we employ a molecule known as titanyl phthalocyanine (TiOPc). Unlike planar phthalocyanine molecules used in our previous works,[31-33] TiOPc has an out-of-plane polar $Ti^{\delta+}=O^{\delta-}$ bond at the center of molecule, which allows molecules to form a slipped stacked structure. Moreover, like other metal phthalocyanines,[34, 39] TiOPc has an in-plane quadrupole moment, which can produce a strong near-field in a nearby 2D crystal. When TiOPc molecules are deposited on TMDCs or graphite, they adopt a face-on orientation[24, 40, 41] with the oxygen atom pointing up (away from the substrate) in the first molecular layer, and pointing down (towards the substrate) in the second molecular layer. We will refer molecules in the first and second layers to as ‘up’ and ‘down’ sites, respectively (see Fig. 1a). Because the TiOPc bilayer has a slipped stacked structure, an array of alternating up and

down sites[40] is formed. This in turn creates a checkerboard-like electrostatic potential superlattice in MoS_2 that harbors two IX states associated with up and down sites.

TiOPc and similar phthalocyanine molecules form a type-II band alignment with monolayer (ML) MoS_2.[42-45] We verify the type-II band alignment in our samples by using ultraviolet photoelectron spectroscopy (UPS). Figure 1b shows UPS spectra of ML-MoS_2 and TiOPc films with various thicknesses grown on ML-MoS_2. Photoelectrons were collected along the surface normal direction, which corresponds to the Γ-point in the reciprocal space. Energy positions of the MoS_2's VBM at the Γ-point and the TiOPc's highest occupied molecular orbital (HOMO) can be extracted from these spectra. The HOMO position as a function of the film thickness is shown in Fig. 1c (red circle). Other than a small band bending near the interface, the HOMO does not show much variation at larger thicknesses (> 1 nm). The surface work function can be extracted from the secondary electron cutoff (SECO) of these spectra (see Fig. S1, supporting information). The work function of MoS_2 and TiOPc at different film thicknesses is shown in Fig. 1c (green triangle). At very small TiOPc thicknesses (~ 0.2 nm), the work function increases initially as compared to that of the bare MoS_2 (thickness = 0 nm). Then, the work function decreases until the thickness reaches ~ 1 nm, at which the work function becomes steady.

Similar variations in the work function was observed in face-on orientated TiOPc on graphite,[40] which was attributed to the polar nature of TiOPc molecules. At sub-ML thicknesses, all molecules have their electronegative oxygen atom pointing up forming a net dipole pointing down, which causes an increase in the work function. As the thickness increases, the second layer, with the oxygen atom pointing down, begins to form on top of the first layer, which causes a decrease in the work function. At larger thicknesses, the topmost layer can contain both pointing-down and pointing-up molecules, which results in a steady work function for thicknesses larger

than 1 nm. The thickness of two layers of TiOPc is ~ 0.6 nm.[46] In this work, we focus on samples with a 0.8 nm thickness to ensure that most MoS_2 is covered by at least two layers of TiOPc molecules. Although a bilayer TiOPc structure does not contain a net dipole moment, its near field can still produce a periodic potential in the nearby MoS_2.

Using the UPS data, we can determine the band alignment of the heterostructure (Fig. 1d). We assume that the VBM at the K-point is 0.13 eV higher than the VBM at the Γ-point.[47] The lowest unoccupied molecular orbital (LUMO) and conduction band minimum (CBM) are drawn based on the reported transport gap of the two materials.[48-51] In the band diagram, we further indicate various excitonic levels obtained by our time-resolved measurement, as red lines. Separations between excitonic levels and its corresponding LUMO/CBM levels represent exciton binding energies.

Quenching of the photoluminescence (PL) signal from intralayer excitons is often used as an indication for the ultrafast charge transfer (CT) and IX formation in a type-II heterostructure.[52-54] Figure 1e shows the PL spectra of the 0.8 nm TiOPc/MoS_2 sample and its constituents obtained with a continuous-wave excitation wavelength of 633 nm (1.96 eV), which can excite both TiOPc and ML-MoS_2. Three main peaks can be identified in these spectra. The peak at 1.89 eV can be attributed to the A-exciton of ML-MoS_2. A pair of lower energy peaks (1.66 eV and 1.35 eV) can be assigned to TiOPc, which is similar to those observed in phase-I TiOPc (also known as β-phase) grown on WSe_2.[41] Compared to Ref. [[41]], our peaks are blue-shifted, which can be attributed to the very small thickness (0.8 nm) of the TiOPc layer. We have also obtained PL spectra for thicker samples (3 nm, 5 nm) – Fig. S2 in the supporting information. The thicker samples show a pair of peaks at 1.55 eV and 1.33 eV, which is in excellent agreement with Ref. [[41]]. Intensities of all these peaks are quenched by a factor 4 in the heterostructure compared to its constituents. This

quenching can be attributed to sub-ps interfacial CT processes that are commonly observed in these type-II heterostructures. Similar PL quenching was reported in VOPc/MoS_2 heterostructures as well.[43, 45]

The dynamic of IX formation and the energy of various IX states are measured by time-resolved two photon photoemission spectroscopy (TR-TPPE). The sample is excited by a visible (1.87 eV) pump pulse and excited electrons are photoionized by a time-delayed probe UV (4.64 eV) pulse. This pump photon energy excites both ML-MoS_2 and TiOPc. For reference, the absorption spectrum of the heterostructure is provided in the supporting information (Fig. S3). Previously, we used the same approach to probe the IX formation in ZnPc/ML-MoS_2 heterostructure.[31] Details on how the spectrum can be interpreted can be found in Ref. [[31]]. Here, we highlight some key observations found in the TiOPc/ML-MoS_2.

Figure 2a shows the spectrum of a 0.8-nm TiOPc on ML-MoS_2 sample. The TPPE intensity is represented by the pseudo-color. The excited state energy (also known as the intermediate state energy) is referenced with respect to the TiOPc's HOMO peak energy. This energy scale (E-E_{HOMO}) corresponds to the exciton energy if the exciton has its hole residing in the TiOPc layer.[31, 55] For instance, the signal at an energy ~ 1.8 eV can be attributed to the TiOPc's singlet (S_1) state.[56] All signal near $t = 0$ is mainly contributed by TiOPc's S_1 excitons because our probe is not sensitive to the intralayer exciton in MoS_2.[31, 57] Indeed, the signal from bare MoS_2 is an order of magnitude weaker (Fig. S4 in the supporting information). We note that the S_1 peak is broad (extending from 1.5 to 2.0 eV), A similar broad S_1 peak is also observed in control experiments done on a thicker TiOPc layer (Fig. S5) and 0.8-nm TiOPc on hBN (Fig. S6), in which only the TiOPc's exciton can be probed. As shown in Fig. 2b, the intensity at ~ 1.8 eV decays rapidly for the 0.8-nm sample, but it decays slower at larger TiOPc thicknesses (e.g., 5 nm). The initial rapid decay in the signal for

the ultrathin sample can be attributed to the ET from TiOPc to the underlying materials[31, 55, 58, 59] because the ET depopulates the S_1 exciton state. A fit of the fast decay component to an exponential function (dashed line) reveals a time constant of ~ 350 fs. The ET time is a bit slower compared to the typical ET time (~ 100 fs) observed in similar molecule/TMDC heterostructures.[31, 43, 44, 57] Figure 2c shows the TPPE spectra of the 0.8 nm sample collected at various delay times (t). As mentioned above, the signal at ~ 1.8 eV quenches rapidly in the first 0.3 ps. At t ~ 0.5 – 1 ps, only a single peak at ~ 1.56 eV is observed (labeled as IX_u), which is assigned to the IX. For t > 0.5 ps, most TiOPc's S_1 excitons are quenched as the ~1.8 eV shoulder is absent. For comparison, the spectrum of the TiOPc/hBN sample exhibits the high energy shoulder at all delay times (see Fig. S6). Finally, we note that the IX can also be produced by hole transfer from MoS_2 to TiOPc. However, we cannot determine the hole transfer time because 1) our probe is not sensitive to intralayer excitons in MoS_2; 2) the spectral overlapping between S_1 and IX_u peaks avoids us to determine the IX_u rise time.

While sub-ps ET and IX formation are also observed in our earlier work on ZnPc/ML-MoS_2,[31] a unique feature can be found in the TiOPc/ML-MoS_2's TR-TPPE spectrum on the ~10 ps timescale. Figure 2d shows the 2D spectral map of the 0.8 nm TiOPc/ML-MoS_2 sample for larger times. The intensity of the original IX peak (IX_u) decreases with increasing time, while another peak at a lower energy (~1.46 eV) emerges (labelled as IX_d). The gradual transfer of the intensity from IX_u to IX_d can also be observed by plotting spectra at different times (Fig. 2e). The observed energy relaxation can be attributed to the IX hopping to lower energy sites. Energy relaxation on this timescale is not observed in ZnPc/ML-MoS_2 conducted under the same experimental condition (Fig. S7 in the supporting information). The major difference between TiOPc and ZnPc is that TiOPc has a permanent dipole at the center of the molecule, which results

in the formation of a slipped stacked structure as illustrated in Fig. 1a. This structure can produce a periodic electrostatic potential in the ML-MoS_2. We propose that this periodic potential can spatially localize the electron in MoS_2 at sites where the potential is minimum, which results in the observed energy relaxation process. Similar exciton localization process has been observed for monolayer $MoSe_2$ in the presence of the moiré potential created by a nearby twisted hBN bilayer.[60]

To demonstrate that an array of molecular dipoles can induce periodic electron trapping sites, we use DFT calculations to determine the electrostatic potential created by the TiOPc bilayer. The atomic structure for bilayer TiOPc, as shown in Fig. 3a and b, is adopted from the molecular crystal structure[61] from the Cambridge Structural Database.[62] Although the centrosymmetric TiOPc bilayer has a zero total polarization, its near-field electrostatic effects can be significant[34, 63] at a distance comparable to the interlayer spacing (a few angstroms). Since the CBM of the ML-MoS_2 at K point is mainly contributed from the Mo d_z^2 orbital,[64] the electrostatic potential modulation from the molecular bilayer is calculated and averaged for distances within 5.68 ± 0.78 Å from the Ti atom in the bottom TiOPc layer, where 5.68 and 0.78 Å correspond to the location of the plane of Mo atoms, and half of the vertical distance between Mo and S atoms, respectively.

As shown in Fig. 3a and in Fig. 3c, the molecular bilayer generates an electrostatic potential superlattice for electrons in the MoS_2. Hence, an electron locating at positions where the potential is negative will have a low potential energy. A potential valley can be found at the down site. On the other hand, the electrostatic potential is higher at the up site. We note that the deep potential valley at the down site is mainly contributed by electropositive H-atoms at the peripheral of the phthalocyanine ring rather than the out-of-plane Ti=O bond. This potential superlattice produces two types of sites for IX – one with a lower energy (down sites) and another one with a higher energy (up sites).

The peak-to-peak electrostatic potential modulation defined as the difference between the maximum and minimum potentials is about 0.092 V. In our experiment, the energy difference between the IX_d and IX_u states is around 0.1 eV, which agrees well with the calculated potential difference. The potential superlattice, as found in other 2D heterostructures,[60, 65] can modulate the band-edge energy for adjacent 2D materials consistent with the in-plane change of the electrostatic potential, which in turn provides trapping sites for excitons. We propose that the IX_u state shown in Fig. 2b corresponds to IXs located at up sites (the potential crest in Fig. 3). This IX state can be populated initially by the CT process because the phthalocyanine ring of the TiOPc molecule at the up site is located right next to the MoS_2. This orientation provides a better wave function overlapping between TiOPc and MoS_2 for CT to occur. Moreover, the smaller energy difference between the intralayer exciton and the IX_u (as compared to the IX_d) can allow the CT process to populate the IX_u preferentially. Then, the IX can diffuse to a neighboring down site where the electron in the MoS_2 can be localized by the potential valley. Such relaxation process requires the IX to hop in the in-plane direction, which should be limited by the hole mobility in the TiOPc layer. For TiOPc films with a face-on orientation, the in-plane mobility at room temperature was reported to be ~ 10^{-2} cm^2/Vs.[66] Using the Einstein relationship, the diffusion constant (D) can be found to be 2.6×10^{-4} cm^2 s^{-1}. For 2D diffusion and a hopping distance of ~ 1 nm, $D \sim 2.6 \times 10^{-4}$ cm^2 s^{-1} corresponds to a hole hopping rate of 10^{11} s^{-1}. This rate agrees roughly with the relaxation time (~ 10 ps) observed in Fig. 2d-e.

For comparison, the electrostatic potential generated by a ML of ZnPc for the Mo atoms in the MoS_2 at 4.62 Å below the Zn atoms is shown in Fig. S8 (supporting information). The atomic structure of ZnPc on MoS_2 from our previous work is used.[67, 68] We note that although the ZnPc layer can also produce potential superlattice in the nearby MoS_2, there are two qualitative

differences in the potential landscape as compared to that in TiOPc/MoS_2. First, the potential superlattice shows a deep potential valley right below the center of each ZnPc molecule. Hence, the IX will be pinned spatially at the molecule after the initial CT process. Second, because the ZnPc lattice does not have the slipped stacked structure, molecules in the second layer are located right on top of molecules in the first layer. Therefore, unlike TiOPc, there is only one type of IX site in the ZnPc/MoS_2. Hence, it cannot produce alternating low and high energy sites for the IX.

Finally, because the TiOPc lattice is incommensurate with the MoS_2 lattice, a moiré pattern is expected to form. To probe whether this moiré pattern is important, we performed a series of DFT calculations using a single TiOPc molecule located in different positions above the MoS_2 layer. As shown in Fig. S9 (supporting information), the CBM levels of MoS_2 remain unchanged, while the HOMO levels shift less than 0.03 eV in these different configurations, indicating that the moiré pattern will have minimal effects on the IX energy.

In this work, the energy and dynamic of IXs in the TiOPc/ML-MoS_2 heterostructure are investigated. Our TR-TPPE measurement shows that two IX states with an energy difference of about 0.1 eV can be formed. Based on the DFT calculation, we argue that these two IX states originate from the modulation of the electrostatic potential in the MoS_2 produced by the near-field electrostatic effects of the molecular layer. Our investigation reveals that such modulating electrostatic potential can spatially localize electrons in the MoS_2. Because the symmetry and size of these molecules can be changed readily, the molecules/2D heterostructure provides a promising platform for untuning the electronic structure of artificial exciton and electron lattices.

Figures and captions:

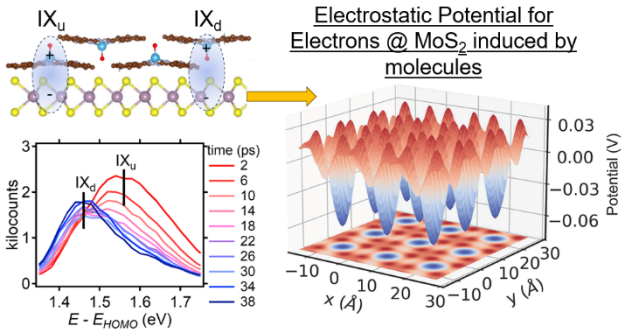

TOC figure

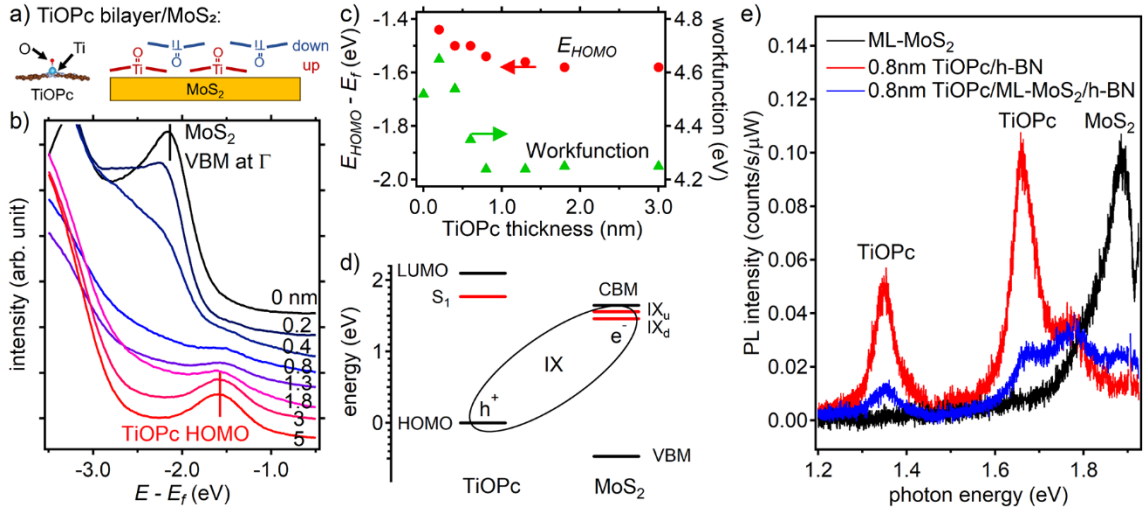

Figure 1: (a) A schematic illustrates a TiOPc bilayer structure on MoS_2. The first and second layers have the oxygen atom pointing up and down, respectively, which we define as "up" and "down" sites in the figure. (b) The UPS spectra of the bare ML-MoS_2, and TiOPc films deposited on the ML-MoS_2. The nominal thickness of the TiOPc layer is shown on the label of each curve. (c) The position of the TiOPc's HOMO (left) and the sample work function (right) as a function of the TiOPc thickness. (d) The energy level diagram of the heterostructure drawn based on the measured HOMO-VBM offset and the transport gap reported in the literature. The HOMO position of TiOPc obtained from the 0.8 nm sample and the VBM position of ML-MoS_2 obtained from the bare MoS_2 sample are used. The excitonic levels measured in our TR-TPPE experiment are shown as the red line. (e) The PL spectra for the heterostructure (blue line) and its constituents (black – ML-MoS_2; red – TiOPc).

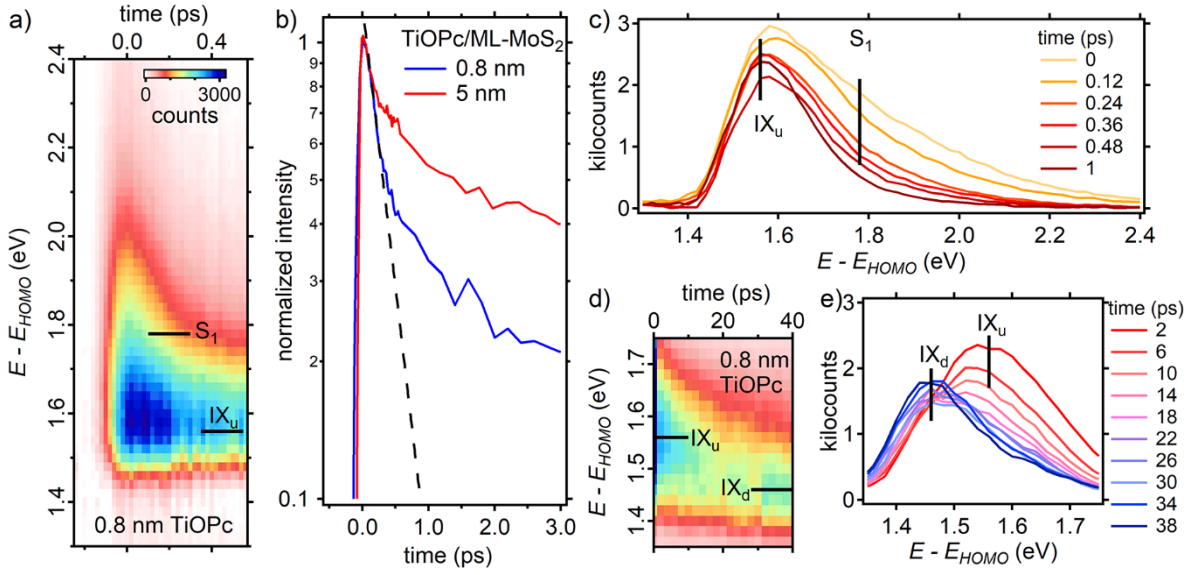

Figure 2: (a) The TR-TPPE 2D-spectral map of the 0.8-nm TiOPc/ML-MoS_2 sample at short delay times. (b) The normalized intensity at the energy corresponding to the TiOPc's S_1 state for the thin (0.8 nm) and thick (5 nm) TiOPc samples. The additional fast intensity decay near time-zero for the 0.8-nm sample can be attributed to the electron transfer from TiOPc to MoS_2. An exponential fit (dashed line) shows a transfer time of ~ 350 fs. (c) The spectra of the 0.8-nm sample at various delay times. (d) The TR-TPPE 2D-spectral map of the 0.8-nm sample at longer delay times. Spectra at various delay times are shown in (e). Two IX states (labelled as IX_u and IX_d) can be identified.

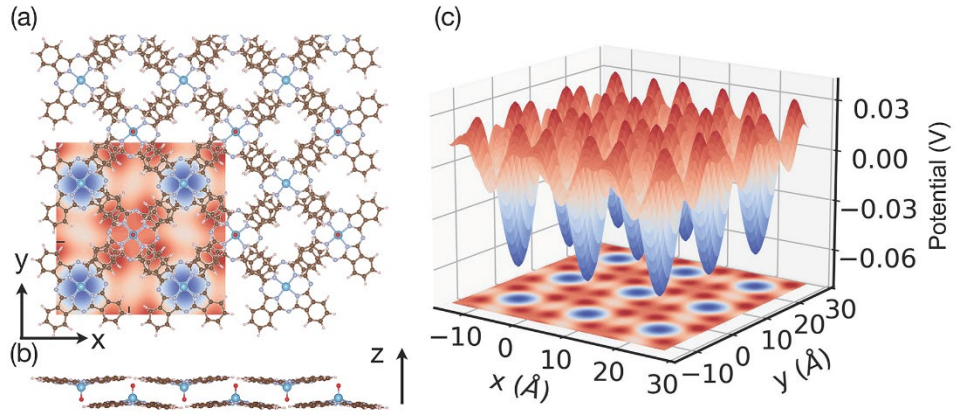

Figure 3: (a) Top view, and (b) side view of the atomic structure of bilayer TiOPc. A color map is overlaid on top of the structure to indicate the electrostatic potential for electrons as a function of the position. (c) The electrostatic potential for electrons from bilayer TiOPc at the position of Mo atoms, which is about 5.68 Å below the Ti atoms of the bottom TiOPc layer.

Supporting Information. Details on experimental and simulation methods. Additional optical and photoemission spectra from control experiments. Experimental and simulation data from the ZnPc/ML-MoS_2 heterostructure. The band alignment determined by DFT calculations.

Acknowledgement:

This work is primarily supported by US National Science Foundation Grant No. DMR-2109979, DMR-2401141. W. –L. C. also acknowledges the support from University of Kansas General Research Fund (2151080). H.Z is supported by the U.S. Department of Energy (DOE), Office of Basic Energy Sciences, Division of Materials Sciences and Engineering under Award No. DE-SC0020995. Q.Z. acknowledges the computational resources at Argonne National Laboratory. Work performed at the Center for Nanoscale Materials, a U.S. Department of Energy Office of Science User Facility, was supported by the U.S. DOE, Office of Basic Energy Sciences, under Contract No. DE-AC02-06CH11357. H. P. acknowledges the computational resources of the National Energy Research Scientific Computing Center, a DOE Office of Science User Facility supported by the Office of Science of the U.S. Department of Energy under Contract No. DE-AC02-05CH11231 using NERSC award BES-ERCAP0028882. F.R. acknowledges scholarship support from Jazan University.

References:

(1) Dean, C. R.; Wang, L.; Maher, P.; Forsythe, C.; Ghahari, F.; Gao, Y.; Katoch, J.; Ishigami, M.; Moon, P.; Koshino, M.; Taniguchi, T.; Watanabe, K.; Shepard, K. L.; Hone, J.; Kim, P. Hofstadter's butterfly and the fractal quantum Hall effect in moire superlattices. *Nature* **2013**, *497*, 598-602.
(2) Hunt, B.; Sanchez-Yamagishi, J. D.; Young, A. F.; Yankowitz, M.; LeRoy, B. J.; Watanabe, K.; Taniguchi, T.; Moon, P.; Koshino, M.; Jarillo-Herrero, P.; Ashoori, R. C. Massive Dirac Fermions and Hofstadter Butterfly in a van der Waals Heterostructure. *Science* **2013**, *340*, 1427-1430.
(3) Ponomarenko, L. A.; Gorbachev, R. V.; Yu, G. L.; Elias, D. C.; Jalil, R.; Patel, A. A.; Mishchenko, A.; Mayorov, A. S.; Woods, C. R.; Wallbank, J. R.; Mucha-Kruczynski, M.; Piot, B. A.; Potemski, M.; Grigorieva, I. V.; Novoselov, K. S.; Guinea, F.; Fal'ko, V. I.; Geim, A. K. Cloning of Dirac fermions in graphene superlattices. *Nature* **2013**, *497*, 594-597.
(4) Cao, Y.; Fatemi, V.; Fang, S.; Watanabe, K.; Taniguchi, T.; Kaxiras, E.; Jarillo-Herrero, P. Unconventional superconductivity in magic-angle graphene superlattices. *Nature* **2018**, *556*, 43-50.
(5) Rivera, P.; Schaibley, J. R.; Jones, A. M.; Ross, J. S.; Wu, S. F.; Aivazian, G.; Klement, P.; Seyler, K.; Clark, G.; Ghimire, N. J.; Yan, J. Q.; Mandrus, D. G.; Yao, W.; Xu, X. D. Observation

of long-lived interlayer excitons in monolayer MoSe2-WSe2 heterostructures. *Nat. Commun.* **2015**, *6*, 6242.
(6) Jin, C. H.; Kim, J.; Utama, M. I. B.; Regan, E. C.; Kleemann, H.; Cai, H.; Shen, Y. X.; Shinner, M. J.; Sengupta, A.; Watanabe, K.; Taniguchi, T.; Tongay, S.; Zettl, A.; Wang, F. Imaging of pure spin-valley diffusion current in WS2-WSe2 heterostructures. *Science* **2018**, *360*, 893-896.
(7) Jauregui, L. A.; Joe, A. Y.; Pistunova, K.; Wild, D. S.; High, A. A.; Zhou, Y.; Scuri, G.; De Greve, K.; Sushko, A.; Yu, C. H.; Taniguchi, T.; Watanabe, K.; Needleman, D. J.; Lukin, M. D.; Park, H.; Kim, P. Electrical control of interlayer exciton dynamics in atomically thin heterostructures. *Science* **2019**, *366*, 870-875.
(8) Seyler, K. L.; Rivera, P.; Yu, H. Y.; Wilson, N. P.; Ray, E. L.; Mandrus, D. G.; Yan, J. Q.; Yao, W.; Xu, X. D. Signatures of moire-trapped valley excitons in MoSe2/WSe2 heterobilayers. *Nature* **2019**, *567*, 66-70.
(9) Tran, K.; Moody, G.; Wu, F. C.; Lu, X. B.; Choi, J.; Kim, K.; Rai, A.; Sanchez, D. A.; Quan, J. M.; Singh, A.; Embley, J.; Zepeda, A.; Campbell, M.; Autry, T.; Taniguchi, T.; Watanabe, K.; Lu, N. S.; Banerjee, S. K.; Silverman, K. L.; Kim, S.; Tutuc, E.; Yang, L.; MacDonald, A. H.; Li, X. Q. Evidence for moire excitons in van der Waals heterostructures. *Nature* **2019**, *567*, 71-75.
(10) Jin, C. H.; Regan, E. C.; Yan, A. M.; Utama, M. I. B.; Wang, D. Q.; Zhao, S. H.; Qin, Y.; Yang, S. J.; Zheng, Z. R.; Shi, S. Y.; Watanabe, K.; Taniguchi, T.; Tongay, S.; Zettl, A.; Wang, F. Observation of moire excitons in WSe2/WS2 heterostructure superlattices. *Nature* **2019**, *567*, 76-80.
(11) Alexeev, E. M.; Ruiz-Tijerina, D. A.; Danovich, M.; Hamer, M. J.; Terry, D. J.; Nayak, P. K.; Ahn, S.; Pak, S.; Lee, J.; Sohn, J. I.; Molas, M. R.; Koperski, M.; Watanabe, K.; Taniguchi, T.; Novoselov, K. S.; Gorbachev, R. V.; Shin, H. S.; Fal'ko, V. I.; Tartakovskii, A. I. Resonantly hybridized excitons in moire superlattices in van der Waals heterostructures. *Nature* **2019**, *567*, 81-86.
(12) Wu, F. C.; Lovorn, T.; MacDonald, A. H. Theory of optical absorption by interlayer excitons in transition metal dichalcogenide heterobilayers. *Phys. Rev. B* **2018**, *97*, 035306.
(13) Yuan, L.; Zheng, B. Y.; Kunstmann, J.; Brumme, T.; Kuc, A. B.; Ma, C.; Deng, S. B.; Blach, D.; Pan, A. L.; Huang, L. B. Twist-angle-dependent interlayer exciton diffusion in WS2-WSe2 heterobilayers. *Nat. Mater.* **2020**, *19*, 617-623.
(14) Bai, Y. S.; Zhou, L.; Wang, J.; Wu, W. J.; McGilly, L. J.; Halbertal, D.; Lo, C. F. B.; Liu, F.; Ardelean, J.; Rivera, P.; Finney, N. R.; Yang, X. C.; Basov, D. N.; Yao, W.; Xu, X. D.; Hone, J.; Pasupathy, A. N.; Zhu, X. Y. Excitons in strain-induced one-dimensional moire potentials at transition metal dichalcogenide heterojunctions. *Nat. Mater.* **2020**, *19*, 1068-1073.
(15) Wang, Z. F.; Rhodes, D. A.; Watanabe, K.; Taniguchi, T.; Hone, J. C.; Shan, J.; Mak, K. F. Evidence of high-temperature exciton condensation in two-dimensional atomic double layers. *Nature* **2019**, *574*, 76-80.
(16) Byrnes, T.; Wen, K.; Yamamoto, Y. Macroscopic quantum computation using Bose-Einstein condensates. *Phys. Rev. A* **2012**, *85*, 040306.
(17) Yu, H. Y.; Liu, G. B.; Tang, J. J.; Xu, X. D.; Yao, W. Moire excitons: From programmable quantum emitter arrays to spin-orbit-coupled artificial lattices. *Sci. Adv.* **2017**, *3*, e1701696.
(18) Harankahage, D.; Cassidy, J.; Yang, M. R.; Porotnikov, D.; Williams, M.; Kholmicheva, N.; Zamkov, M. Quantum Computing with Exciton Qubits in Colloidal Semiconductor Nanocrystals. *J. Phys. Chem. C* **2021**, *125*, 22195-22203.

(19) Ghosh, S.; Liew, T. C. H. Quantum computing with exciton-polariton condensates. *Npj Quantum Inform* **2020**, *6*, 16.
(20) Jariwala, D.; Marks, T. J.; Hersam, M. C. Mixed-dimensional van der Waals heterostructures. *Nat. Mater.* **2017**, *16*, 170-181.
(21) Huang, Y. L.; Zheng, Y. J.; Song, Z. B.; Chi, D. Z.; Wee, A. T. S.; Quek, S. Y. The organic-2D transition metal dichalcogenide heterointerface. *Chem. Soc. Rev.* **2018**, *47*, 3241-3264.
(22) Wang, H. M.; Li, C. H.; Fang, P. F.; Zhang, Z. L.; Zhang, J. Z. Synthesis, properties, and optoelectronic applications of two-dimensional MoS2 and MoS2-based heterostructures. *Chem. Soc. Rev.* **2018**, *47*, 6101-6127.
(23) Padgaonkar, S.; Amsterdam, S. H.; Bergeron, H.; Su, K.; Marks, T. J.; Hersam, M. C.; Weiss, E. A. Molecular-Orientation-Dependent Interfacial Charge Transfer in Phthalocyanine/MoS2 Mixed-Dimensional Heterojunctions. *J. Phys. Chem. C* **2019**, *123*, 13337-13343.
(24) Park, J. H.; Sanne, A.; Guo, Y. Z.; Amani, M.; Zhang, K. H.; Movva, H. C. P.; Robinson, J. A.; Javey, A.; Robertson, J.; Banerjee, S. K.; Kummel, A. C. Defect passivation of transition metal dichalcogenides via a charge transfer van der Waals interface. *Sci. Adv.* **2017**, *3*, 1701661.
(25) Zhu, T.; Yuan, L.; Zhao, Y.; Zhou, M. W.; Wan, Y.; Mei, J. G.; Huang, L. B. Highly mobile charge-transfer excitons in two-dimensional WS2/tetracene heterostructures. *Sci. Adv.* **2018**, *4*, 3104.
(26) Cui, X. X.; Han, D.; Guo, H. L.; Zhou, L. W.; Qiao, J. S.; Liu, Q.; Cui, Z. H.; Li, Y. F.; Lin, C. W.; Cao, L. M.; Ji, W.; Petek, H.; Feng, M. Realizing nearly-free-electron like conduction band in a molecular film through mediating intermolecular van der Waals interactions. *Nat. Commun.* **2019**, *10*, 3374.
(27) Park, S.; Mutz, N.; Kovalenko, S. A.; Schultz, T.; Shin, D.; Aljarb, A.; Li, L. J.; Tung, V.; Amsalem, P.; List-Kratochvil, E. J. W.; Stahler, J.; Xu, X. M.; Blumstengel, S.; Koch, N. Type-I Energy Level Alignment at the PTCDA-Monolayer MoS2 Interface Promotes Resonance Energy Transfer and Luminescence Enhancement. *Adv. Sci.* **2021**, *8*, 2100215.
(28) Ye, L.; Xu, X. H.; He, S. Y.; Liu, Y. P.; Jin, Y. Z.; Yang, Y. M.; Zhu, H. M. Molecular Triplet Sensitization of Monolayer Semiconductors in 2D Organic/Inorganic Hybrid Heterostructures. *ACS Nano* **2022**, *16*, 12532-12540.
(29) Gobbi, M.; Bonacchi, S.; Lian, J. X.; Vercouter, A.; Bertolazzi, S.; Zyska, B.; Timpel, M.; Tatti, R.; Olivier, Y.; Hecht, S.; Nardi, M. V.; Beljonne, D.; Orgiu, E.; Samorì, P. Collective molecular switching in hybrid superlattices for light-modulated two-dimensional electronics. *Nat. Commun.* **2018**, *9*, 2661.
(30) Gobbi, M.; Bonacchi, S.; Lian, J. X.; Liu, Y.; Wang, X. Y.; Stoeckel, M. A.; Squillaci, M. A.; D'Avino, G.; Narita, A.; Mullen, K.; Feng, X. L.; Olivier, Y.; Beljonne, D.; Samori, P.; Orgiu, E. Periodic potentials in hybrid van der Waals heterostructures formed by supramolecular lattices on graphene. *Nat. Commun.* **2017**, *8*, 14767.
(31) Kafle, T. R.; Kattel, B.; Yao, P.; Zereshki, P.; Zhao, H.; Chan, W. L. Effect of the Interfacial Energy Landscape on Photoinduced Charge Generation at the ZnPc/MoS2 Interface. *J. Am. Chem. Soc.* **2019**, *141*, 11328-11336.
(32) Kafle, T. R.; Kattel, B.; Lane, S. D.; Wang, T.; Zhao, H.; Chan, W. L. Charge Transfer Exciton and Spin Flipping at Organic-Transition-Metal Dichalcogenide Interfaces. *ACS Nano* **2017**, *11*, 10184-10192.

(33) Rijal, K.; Amos, S.; Valencia-Acuna, P.; Rudayni, F.; Fuller, N.; Zhao, H.; Peelaers, H.; Chan, W. L. Nanoscale Periodic Trapping Sites for Interlayer Excitons Built by Deformable Molecular Crystal on 2D Crystal. *ACS Nano* **2023**, *17*, 7775-7786.
(34) Zhou, Q.; Anaclet, B.; Steiner, T.; Kotiuga, M.; Darancet, P. Engineering the Electronic Structure of Two-Dimensional Materials with Near-Field Electrostatic Effects of Self-Assembled Organic Layers. *arxiv* **2021**, arXiv:2109.09990
(35) Li, H. Y.; Li, S. W.; Regan, E. C.; Wang, D. Q.; Zhao, W. Y.; Kahn, S.; Yumigeta, K.; Blei, M.; Taniguchi, T.; Watanabe, K.; Tongay, S.; Zettl, A.; Crommie, M. F.; Wang, F. Imaging two-dimensional generalized Wigner crystals. *Nature* **2021**, *597*, 650-654.
(36) Regan, E. C.; Wang, D. Q.; Jin, C. H.; Utama, M. I.; Gao, B. N.; Wei, X.; Zhao, S. H.; Zhao, W. Y.; Zhang, Z. C.; Yumigeta, K.; Blei, M.; Carlstrom, J. D.; Watanabe, K.; Taniguchi, T.; Tongay, S.; Crommie, M.; Zettl, A.; Wang, F. Mott and generalized Wigner crystal states in WSe2/WS2 moire superlattices. *Nature* **2020**, *579*, 359-363.
(37) Reddy, A. P.; Devakul, T.; Fu, L. Artificial Atoms, Wigner Molecules, and an Emergent Kagome Lattice in Semiconductor Moir′e Superlattices. *Phys. Rev. Lett.* **2023**, *131*, 246501.
(38) Ulman, K.; Quek, S. Y. Organic-2D Material Heterostructures: A Promising Platform for Exciton Condensation and Multiplication. *Nano Lett.* **2021**, *21*, 8888-8894.
(39) Schwarze, M.; Tress, W.; Beyer, B.; Gao, F.; Scholz, R.; Poelking, C.; Ortstein, K.; Gunther, A. A.; Kasemann, D.; Andrienko, D.; Leo, K. Band structure engineering in organic semiconductors. *Science* **2016**, *352*, 1446-1449.
(40) Fukagawa, H.; Yamane, H.; Kera, S.; Okudaira, K. K.; Ueno, N. Experimental estimation of the electric dipole moment and polarizability of titanyl phthalocyanine using ultraviolet photoelectron spectroscopy. *Phys. Rev. B* **2006**, *73*, 041302.
(41) Xiong, S.; Wang, Y.; Yao, J.; Xu, J.; Xu, M. Exciton Dynamics of TiOPc/WSe2 Heterostructure. *ACS Nano* **2024**, *18*, 10249-10258.
(42) Choudhury, P.; Ravavarapu, L.; Dekle, R.; Chowdhury, S. Modulating Electronic and Optical Properties of Monolayer MoS2 Using Nonbonded Phthalocyanine Molecules. *J. Phys. Chem. C* **2017**, *121*, 2959-2967.
(43) Wang, Z. K.; Sun, C.; Xu, X. H.; Liu, Y. P.; Chen, Z.; Yang, Y.; Zhu, H. M. Long-Range Hot Charge Transfer Exciton Dissociation in an Organic/2D Semiconductor Hybrid Excitonic Heterostructure. *J. Am. Chem. Soc.* **2023**, *145*, 11227-11235.
(44) Schwinn, M. C.; Rafiq, S.; Lee, C. M.; Bland, M. P.; Song, T. W.; Sangwan, V. K.; Hersam, M. C.; Chen, L. X. Charge transfer dynamics and interlayer exciton formation in MoS2/VOPc mixed dimensional heterojunction. *J. Chem. Phys.* **2022**, *157*, 184701.
(45) Kong, Y. H.; Obaidulla, S. M.; Habib, M. R.; Wang, Z. K.; Wang, R.; Khan, Y. Y.; Zhu, H. M.; Xu, M. S.; Yang, D. R. Interlayer exciton emission in a MoS/VOPc inorganic/organic van der Waals heterostructure. *Materials Horizons* **2022**, *9*, 1253-1263.
(46) Okada, O.; Klein, M. L. Molecular dynamics studies of titanylphthalocyanine crystals. *J Chem Soc Faraday T* **1996**, *92*, 2463-2467.
(47) Jin, W. C.; Yeh, P. C.; Zaki, N.; Zhang, D. T.; Sadowski, J. T.; Al-Mahboob, A.; van der Zande, A. M.; Chenet, D. A.; Dadap, J. I.; Herman, I. P.; Sutter, P.; Hone, J.; Osgood, R. M. Direct Measurement of the Thickness-Dependent Electronic Band Structure of MoS2 Using Angle-Resolved Photoemission Spectroscopy. *Phys. Rev. Lett.* **2013**, *111*, 106801.
(48) Gao, W. Y.; Kahn, A. Electronic structure and current injection in zinc phthalocyanine doped with tetrafluorotetracyanoquinodimethane: Interface versus bulk effects. *Org. Electron.* **2002**, *3*, 53-63.

(49) Zahn, D. R. T.; Gavrila, G. N.; Gorgoi, M. The transport gap of organic semiconductors studied using the combination of direct and inverse photoemission. *Chem. Phys.* **2006**, *325*, 99-112.
(50) Hill, I. G.; Kahn, A.; Soos, Z. G.; Pascal, R. A. Charge-separation energy in films of pi-conjugated organic molecules. *Chem. Phys. Lett.* **2000**, *327*, 181-188.
(51) Park, S.; Mutz, N.; Schultz, T.; Blumstengel, S.; Han, A.; Aljarb, A.; Li, L. J.; List-Kratochvil, E. J. W.; Amsalem, P.; Koch, N. Direct determination of monolayer MoS2 and WSe2 exciton binding energies on insulating and metallic substrates. *2D Mater.* **2018**, *5*, 025003.
(52) Fang, H.; Battaglia, C.; Carraro, C.; Nemsak, S.; Ozdol, B.; Kang, J. S.; Bechtel, H. A.; Desai, S. B.; Kronast, F.; Unal, A. A.; Conti, G.; Conlon, C.; Palsson, G. K.; Martin, M. C.; Minor, A. M.; Fadley, C. S.; Yablonovitch, E.; Maboudian, R.; Javey, A. Strong interlayer coupling in van der Waals heterostructures built from single-layer chalcogenides. *Proceedings of the National Academy of Sciences of the United States of America* **2014**, *111*, 6198-6202.
(53) Hong, X. P.; Kim, J.; Shi, S. F.; Zhang, Y.; Jin, C. H.; Sun, Y. H.; Tongay, S.; Wu, J. Q.; Zhang, Y. F.; Wang, F. Ultrafast charge transfer in atomically thin MoS2/WS2 heterostructures. *Nat. Nanotechnol.* **2014**, *9*, 682-686.
(54) Ceballos, F.; Bellus, M. Z.; Chiu, H. Y.; Zhao, H. Ultrafast Charge Separation and Indirect Exciton Formation in a MoS2-MoSe2 van der Waals Heterostructure. *ACS Nano* **2014**, *8*, 12717-12724.
(55) Wang, T.; Kafle, T. R.; Kattel, B.; Chan, W.-L. A Multidimensional View of Charge Transfer Excitons at Organic Donor–Acceptor Interfaces. *J. Am. Chem. Soc.* **2017**, *139*, 4098-4106.
(56) Wang, T.; Kafle, T. R.; Kattel, B.; Chan, W. L. Observation of an Ultrafast Exciton Hopping Channel in Organic Semiconducting Crystals. *J. Phys. Chem. C* **2016**, *120*, 7491-7499.
(57) Rijal, K.; Rudayni, F.; Kafle, T. R.; Chan, W.-L. Collective Effects of Band Offset and Wave Function Dimensionality on Impeding Electron Transfer from 2D to Organic Crystals. *J. Phys. Chem. Lett.* **2020**, *11*, 7495-7501.
(58) Wanigasekara, S.; Rijal, K.; Rudayni, F.; Panth, M.; Shultz, A.; Wu, J. Z.; Chan, W. L. Using an Atomically Thin Layer of Hexagonal Boron Nitride to Separate Bound Charge-Transfer Excitons at Organic Interfaces. *Phys. Rev. Appl.* **2022**, *18*, 014042.
(59) Wang, T.; Liu, Q. F.; Caraiani, C.; Zhang, Y. P.; Wu, J.; Chan, W. L. Effect of Interlayer Coupling on Ultrafast Charge Transfer from Semiconducting Molecules to Mono- and Bilayer Graphene. *Phys. Rev. Appl.* **2015**, *4*, 014016.
(60) Kim, D. S.; Dominguez, R. C.; Mayorga-Luna, R.; Ye, D. Y.; Embley, J.; Tan, T. X.; Ni, Y.; Liu, Z. D.; Ford, M.; Gao, F. Y.; Arash, S.; Watanabe, K.; Taniguchi, T.; Kim, S.; Shih, C. K.; Lai, K. J.; Yao, W.; Yang, L.; Li, X. Q.; Miyahara, Y. Electrostatic moire potential from twisted hexagonal boron nitride layers. *Nat. Mater.* **2024**, *23*, 65-70.
(61) Oka, K.; Okada, O.; Nukada, K. Study of the Crystal-Structure of Titanylphthalocyanine by Rietveld Analysis and Intermolecular Energy Minimization Method. *Jpn J Appl Phys 1* **1992**, *31*, 2181-2184.
(62) Groom, C. R.; Bruno, I. J.; Lightfoot, M. P.; Ward, S. C. The Cambridge Structural Database. *Acta Crystallographica Section B-Structural Science Crystal Engineering and Materials* **2016**, *72*, 171-179.
(63) Natan, A.; Kronik, L.; Haick, H.; Tung, R. T. Electrostatic properties of ideal and non-ideal polar organic monolayers: Implications for electronic devices. *Adv. Mater.* **2007**, *19*, 4103-4117.
(64) Zollner, K.; Faria, P. E.; Fabian, J. Strain-tunable orbital, spin-orbit, and optical properties of monolayer transition-metal dichalcogenides. *Phys. Rev. B* **2019**, *100*, 195126.

(65) Zhao, P.; Xiao, C. X.; Yao, W. Universal superlattice potential for 2D materials from twisted interface inside h-BN substrate. *Npj 2d Materials and Applications* **2021**, *5*, 38.
(66) Zhang, Y.; Wei, X. C.; Zhang, H.; Chen, X.; Wang, J. Ambipolar organic transistors with high on/off ratio by introducing a modified layer of gate insulator. *Appl. Surf. Sci.* **2018**, *427*, 452-457.
(67) Zhou, Q. F.; Liu, Z. F.; Marks, T. J.; Darancet, P. Range-separated hybrid functionals for mixed dimensional heterojunctions: Application to phthalocyanines/MoS. *Apl Mater* **2021**, *9*, 121112.
(68) Amsterdam, S. H.; Stanev, T. K.; Wang, L. Q.; Zhou, Q. F.; Irgen-Gioro, S.; Padgaonkar, S.; Murthy, A. A.; Sangwan, V. K.; Dravid, V. P.; Weiss, E. A.; Darancet, P.; Chan, M. K. Y.; Hersam, M. C.; Stern, N. P.; Marks, T. J. Mechanistic Investigation of Molybdenum Disulfide Defect Photoluminescence Quenching by Adsorbed Metallophthalocyanines. *J. Am. Chem. Soc.* **2021**, *143*, 17153-17161.